

Drug Delivery

 International Edition: DOI: 10.1002/anie.201801984
 German Edition: DOI: 10.1002/ange.201801984

Polymeric Nanoparticles with a Glutathione-Sensitive Heterodimeric Multifunctional Prodrug for In Vivo Drug Monitoring and Synergistic Cancer Therapy

Fuwu Zhang, Qianqian Ni, Orit Jacobson, Siyuan Cheng, Arthur Liao, Zhantong Wang, Zhimei He, Guocan Yu, Jibin Song, Ying Ma, Gang Niu, Longjiang Zhang,* Guizhi Zhu,* and Xiaoyuan Chen*

Abstract: Polymeric micelle-based drug delivery systems have dramatically improved the delivery of small molecular drugs, yet multiple challenges remain to be overcome. A polymeric nanomedicine has now been engineered that possesses an ultrahigh loading (59%) of a glutathione (GSH)-sensitive heterodimeric multifunctional prodrug (HDMP) to effectively co-deliver two synergistic drugs to tumors. An HDMP comprising of chemotherapeutic camptothecin (CPT) and photosensitizer 2-(1-hexyloxyethyl)-2-devinyl pyropheophorbide-a (HPPH) was conjugated via a GSH-cleavable linkage. The intrinsic fluorogenicity and label-free radio-chelation (^{64}Cu) of HPPH enabled direct drug monitoring by fluorescence imaging and positron emission tomography (PET). Through quantitative PET imaging, HDMP significantly improves drug delivery to tumors. The high synergistic therapeutic efficacy of HDMP-loaded NPs highlights the rational design of HDMP, and presents exciting opportunities for polymer NP-based drug delivery.

Polymeric micellar nanoparticles are one of the most important drug carriers in cancer nanomedicine. Most of these micellar structures consist of a hydrophobic core for drug loading as well as a PEGylated hydrophilic shell for improved colloidal stability and the stealth effects.^[1] Several micellar formulations, for instance, Genexol-PM, NK012, and NK105 have advanced to clinical trials, yet none has been approved in the United States.^[2] Part of the challenges these micellar formulations face are low drug loading capacity, premature drug release, inability of in vivo drug monitoring,

and limited drug accumulation in the tumor tissues.^[3] To address such limitations, various drug carriers have been developed with favorable characteristics towards drug delivery; however, their structural complexities are stumbling blocks for clinical translation.^[3b,4] Alternatively, the payloads, often small molecular drugs, can be engineered to improve the performance of nanotherapeutics.^[5] Compared to drug carrier optimization, the modification of small molecular drugs is relatively simple and could facilitate the process of drug development. Towards this end, dimeric prodrugs are promising candidates with high drug loading capacity and prolonged drug release.^[6]

We report herein the design of GSH-sensitive HDMP that not only has exceptionally high loading efficiency and high loading capacity, entails straightforward PET pharmacoinaging in vivo, but is also able to realize synergistic cancer therapy (Figure 1). As a proof of concept, chemotherapeutic drug CPT and photosensitizer HPPH were chosen and conjugated via a GSH-cleavable disulfide bond. HPPH is a photosensitizing agent that, upon laser irradiation, consumes molecular oxygen to generate singlet oxygen to kill cancer cells.^[7] CPT is a topoisomerase I inhibitor that stabilizes the topoisomerase I-DNA complexes, causing DNA damage and consequently killing cancer cells.^[8] Furthermore, CPT is also reported to be a hypoxia-inducible

[*] Dr. F. Zhang, Q. Ni, Dr. O. Jacobson, S. Cheng, A. Liao, Dr. Z. Wang, Z. He, Dr. G. Yu, Dr. J. Song, Dr. Y. Ma, Dr. G. Niu, Dr. G. Zhu, Dr. X. Chen

Laboratory of Molecular Imaging and Nanomedicine (LOMIN), National Institute of Biomedical Imaging and Bioengineering (NIBIB), National Institutes of Health Bethesda, MD 20892 (USA)
 E-mail: guizhi.zhu@nih.gov
 shawn.chen@nih.gov

Q. Ni, Dr. L. Zhang
 Department of Medical Imaging, Jinling Hospital, Medical School of Nanjing University
 Nanjing, 210002 Jiangsu (China)
 E-mail: kevinzhli@163.com

Supporting information and the ORCID identification number(s) for the author(s) of this article can be found under:
<https://doi.org/10.1002/anie.201801984>

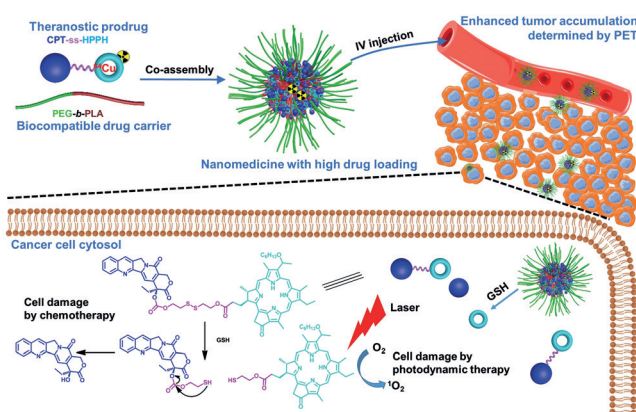


Figure 1. Design of polymer nanotherapeutics with an extremely high loading capacity of GSH-sensitive HDMP, CPT-ss-HPPH, for efficient drug accumulation in tumor and synergistic chemotherapy and photodynamic therapy. This nanotherapeutic system features intrinsic radio-pharmaceutical labeling with ^{64}Cu via direct chelation into HPPH, which enable quantitative pharmacoinaging by PET.

factor-1 α (HIF-1 α) inhibitor that attenuates hypoxia and makes cells vulnerable to low oxygen concentrations.^[9] Therefore, CPT is expected to enhance the cytotoxic effect induced by HPPH. Notably, HPPH itself can serve as a fluorescent dye and a chelator for ⁶⁴Cu labeling, allowing the as-designed HDMP to be directly visualized by fluorescence and PET imaging in vitro and in vivo. Remarkably, the quantitative nature of PET pharmacoinaging enables an accurate monitoring of HDMP and the determination of its pharmacokinetics and biodistribution in vivo. Moreover, the redox-responsive disulfide bond is readily cleavable by the high concentration of GSH in cancer cells, which would release CPT and HPPH from the HDMP through a cascade reaction.

The GSH-sensitive HDMP is synthesized through a simple two-step reaction from commercially available CPT and HPPH (Supporting Information, Scheme S1). In brief, CPT was reacted with 2,2'-dithiodiethanol to produce prodrug CPT-ss-OH. CPT-ss-OH was further reacted with HPPH via ester formation to afford CPT-ss-HPPH, which was confirmed by ESI-MS (Supporting Information, Figure S1) and ¹H NMR (Supporting Information, Figure S2). The UV/Vis spectrum of CPT-ss-HPPH also displayed the characteristic spectra of both CPT and HPPH (Supporting Information, Figure S5). A control CPT-cc-HPPH with a non-cleavable linkage was synthesized in a similar approach (Supporting Information, Scheme S2, Figures S3, S4). We then tested the ability of CPT-ss-HPPH to generate reactive oxygen species (ROS) using anthracene-9,10-dipropionic acid (ADPA) as a ROS indicator (Supporting Information, Figure S6).^[10] The decrease of the absorbance of ADPA at 410 nm indicates the generation of ROS. Both HPPH and CPT-ss-HPPH samples displayed a continuously decreasing absorbance as irradiation time increased. Worth noting is the faster decrease at 410 nm of CPT-ss-HPPH over HPPH samples, which indicates that CPT-ss-HPPH is superior in ROS generation (Supporting Information, Figure S6a–c), likely due to the stabilization of HPPH chemical structure upon conjugation with a CPT-ss-group. Furthermore, the loss of absorbance of HPPH or CPT-ss-HPPH at 662 nm suggests their instability during laser irradiation (Supporting Information, Figure S6a,b). A quantitative analysis by determining the loss of absorbance at 662 nm reveals that nearly 90% of HPPH degraded, in contrast to less than 20% for CPT-ss-HPPH (Supporting Information, Figure S6d,e). These results demonstrate that by conjugating CPT to HPPH, both the photostability and ROS generation capability of HPPH were improved.

We then investigated the drug loading into biocompatible and degradable poly(ethylene glycol)-*block*-poly(D,L-lactic acid) (PEG-*b*-PLA) nanoparticles (Table 1). Owing to its intrinsic aromatic nature, CPT has limited solubility in both aqueous solutions and most organic solvents. Dimethyl sulfoxide (DMSO) is the only common solvent with good solubility for CPT. At a drug/polymer feeding ratio of 4%, the obtained nanoparticle via nanoprecipitation from DMSO to water had a number-averaged hydrodynamic diameter of 430 \pm 86 nm (Table 1, entry 1). The obtained nanoparticles, however, were not stable and precipitated in a few hours. In contrast, at a feeding ratio of 10%, the HPPH loading into

Table 1: Drug loading of CPT, HPPH, CPT-ss-HPPH into PEG-*b*-PLA nanoparticles.

Entry	Drug	Ratio ^[a]	<i>d</i> [nm] ^[b]	LE [%] ^[c]	DL [%] ^[d]
1 ^[e]	CPT	0.04	430 \pm 86	NA	NA
2	HPPH	0.1	35 \pm 9	98	8.9
3	CPT-ss-HPPH	0.2	34 \pm 9	97	16
4	CPT-ss-HPPH	0.4	33 \pm 8	97	28
5	CPT-ss-HPPH	1.0	46 \pm 11	98	49
6 ^[f]	CPT-ss-HPPH	1.5	52 \pm 13	97	59
7	CPT-cc-HPPH	0.2	35 \pm 9	97	16

[a] Feeding ratio of drug/PEG-*b*-PLA. [b] Number-averaged hydrodynamic diameter, as measured by DLS. [c] LE = mass of encapsulated drug/mass of feeding drug. [d] DL = mass of encapsulated drug/total mass of polymer and encapsulated drug. [e] The formulation was not stable, no purification was performed. [f] Few visible precipitates were observed after 3 d. No visible precipitation was observed for formulations in the other entries within 2 weeks.

PEG-*b*-PLA was well controlled with a loading efficiency (LE) as high as 98% and a drug loading capacity (DL) up to 8.9% (Table 1, entry 2). When CPT was linked with HPPH, the hydrophilic hydroxy group from CPT and the hydrophilic carboxylic acid group from HPPH were transformed into hydrophobic carbonate and ester group, respectively, leading to enhanced overall hydrophobicity of CPT-ss-HPPH (0.098 \pm 0.015 μ g mL⁻¹ in water). The increased hydrophobicity of CPT-ss-HPPH was hypothesized to be more efficiently encapsulated into nanocarriers with higher LE and DL than the corresponding monomers. Indeed, when the drug/polymer feeding ratio increased from 0.2 to 1.5, the DL increased from 16% to nearly 60%, with a quantitative LE of 97% (Table 1, entry 3–6). At a 0.2 feeding ratio, the obtained nanoparticles had hydrodynamic diameters of 34 \pm 9 nm, with a nearly neutral zeta potential, which was stable with no visible precipitation and significant change in hydrodynamic diameters for at least a week (Supporting Information, Figures S7, S8). Transmission electron microscopy (TEM) suggested that these nanoparticles were spherical with an average size of 35 \pm 5 nm (Figure 2a). A similar size distribution was found at a drug feeding ratio of 0.4. At higher feeding ratios, their diameters increased to about 50 nm (Table 1, entries 5, 6). As expected, the control CPT-cc-HPPH also had a high LE at a 0.2 drug/polymer feeding ratio (Table 1, entry 7). The exceptional LE and DL of the designed HDMP are highly attractive for translational studies due to their simplicity and effectiveness.

The release of an encapsulated drug from a polymeric micellar formulation is mainly a diffusion-controlled process that depends on several factors, including the intrinsic properties of both carrier and drug, drug distribution over carriers, and releasing environment.^[11] Indeed, one of the prevalent drawbacks of micellar formulations is initial burst drug release, which is often caused by the weakly bound drugs on the nanoparticle surface.^[11a] In our HDMP, the lower aqueous solubility and increased molecular weight over either CPT or HPPH (both ca. 10 μ g mL⁻¹) will likely lead to slower drug release than either of the monomeric drugs.^[11b,12] Additionally, we expect GSH to specifically facilitate drug release from CPT-ss-HPPH by cleaving the disulfide linkage.

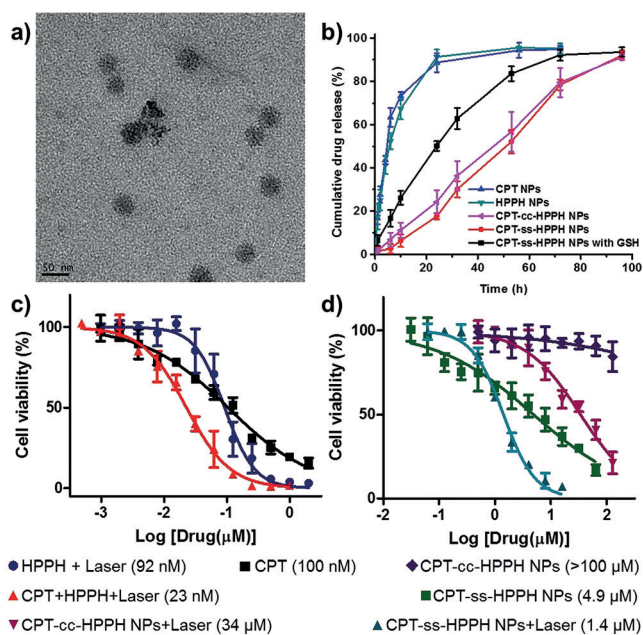


Figure 2. a) A TEM image of CPT-ss-HPPH NPs. b) In vitro drug release in PBS with or without 10 mM GSH at 37°C; c), d) MTT assay results showing the in vitro cytotoxicities of various formulations with or without 671 nm laser irradiations for 1 min at 10 mWcm⁻². The IC₅₀ values are shown in brackets.

Accordingly, we examined the drug release of CPT NPs, HPPH NPs, CPT-cc-HPPH NPs, and CPT-ss-HPPH in PBS for 4 d with and without 10 mM GSH at 37°C (Figure 2b). As expected, the release of CPT and HPPH from nanoparticles was quite fast, resembling most micellar formulations with a release half-life ($t_{1/2}$) of only 4.6 h and 5.6 h, respectively. In contrast, both of our HDMPs, CPT-ss-HPPH and CPT-cc-HPPH, displayed a nearly zero-order release where the drug was released almost at a constant rate. Their $t_{1/2}$ values were determined to be 51 h for CPT-ss-HPPH and 46 h for CPT-cc-HPPH, which are almost 10-fold longer than either monomer. The slow zero-order release is highly desirable for drug delivery since it can reduce premature drug release during blood circulation, and consequently, ameliorate side effects. As mentioned, another important feature of CPT-ss-HPPH is its GSH-sensitive disulfide bond which allows HPPH and intact CPT to be released through a two-step of cascade reaction (Figure 1). This feature was demonstrated by our observation that 10 mM GSH indeed led to a much faster drug release with a $t_{1/2}$ of only 24 h (Figure 2b). The significantly decreased $t_{1/2}$ in the presence of GSH (24 h vs. 51 h) would allow for effective drug activation and release upon internalization into cells, thereby permitting efficient cell killing by CPT-ss-HPPH. Furthermore, we studied the CPT release from CPT-ss-HPPH NPs via an incubation method and monitored the concentration of released CPT over time (Supporting Information, Figure S9). As anticipated, the CPT concentration increased over time, reaching a 67% accumulative release over 48 h. Together, these drug release studies demonstrated that our GSH-sensitive HDMP NPs are a well-controlled responsive drug release system.

Encouraged by the incredible drug loading and release properties, we then investigated in vitro cytotoxicities of these formulations on HCT116 human colon cancer cells (Figure 2c,d). First, the fluorogenicity of HPPH was harnessed to investigate the in vitro cellular uptake of our HDMPs and HPPH. As shown in the Supporting Information, Figure S10, both HDMP-loaded NPs were internalized into cells as efficiently as HPPH NPs. We then measured the cytotoxicities of free CPT, HPPH, and their 1:1 mixture. The IC₅₀ of HPPH and CPT were determined to be 92 nM and 100 nM, respectively, while the IC₅₀ of the combination dropped to 23 nM (Figure 2c). The combination index (CI) was calculated to be 0.49, which indicated high synergy between CPT and HPPH. Similar CI values were obtained at IC₂₅, IC₇₅, and IC₉₀ (Supporting Information, Table S1). The synergistic effects of CPT and HPPH were also verified on U87MG and 4T1 cancer cells with CI values of 0.33 and 0.41, respectively (Supporting Information, Figure S11). The strong synergy is probably a combined result of their different mechanisms of cell killing and the fact that CPT rendered the cells vulnerable to low oxygen levels caused by laser irradiation of HPPH. Owing to relatively slow release, CPT-ss-HPPH NPs showed much lower in vitro cytotoxicity in the absence of laser irradiation (IC₅₀: 4.9 μM) than either of monomeric drugs, and the non-responsive CPT-cc-HPPH NPs showed marginal in vitro cytotoxicity (IC₅₀ > 100 μM), indicating the critical role of the disulfide bond in the activation of therapeutic efficacy of CPT-ss-HPPH. Additional laser irradiation of cells treated with CPT-ss-HPPH NPs enhanced the cytotoxicity, with IC₅₀ decreased from 4.9 μM to 1.4 μM. If we assume the laser-induced cytotoxicity of CPT-ss-HPPH was close to that of CPT-cc-HPPH (IC₅₀: 34 μM), the CI of CPT and HPPH in CPT-ss-HPPH would be 0.33. The necessity of GSH-responsive disulfide was also confirmed on U87MG and 4T1 cancer cells, where significantly reduced IC₅₀ values of CPT-ss-HPPH NPs were observed over non-cleavable counterparts (Supporting Information, Figure S11).

We then studied HDMP-loaded NPs for drug delivery into tumor in mice. One of the most interesting features of our HPPH-based HDMPs is their capability of intrinsic radio-pharmaceutical labeling with isotopes such as ⁶⁴Cu, which enables quantitative pharmacoinaging to monitor drug distribution in vivo by PET imaging. As shown in Figure 3a, compared with HPPH, significantly more CPT-ss-HPPH was accumulated in tumor at each corresponding time point. The quantification of decay-corrected PET images demonstrated that the tumor accumulation of CPT-ss-HPPH reached 6.0 ± 0.6% ID g⁻¹ at 24 h post-injection and remained high at 6.1 ± 0.8% ID g⁻¹ at 48 h, while that of HPPH was only 2.8 ± 0.8% ID g⁻¹ at 48 h (Figure 3b). The significant higher tumor accumulation of CPT-ss-HPPH than HPPH was confirmed by ex vivo biodistribution based on γ-counting of excised organs (Figure 3c). Since the nanocarriers for both HPPH and CPT-ss-HPPH were the same with indistinguishable sizes, the significantly higher accumulation of CPT-ss-HPPH over HPPH was attributed to the much slower premature release of CPT-ss-HPPH during blood circulation as well as higher retention in tumor. Note that the slow

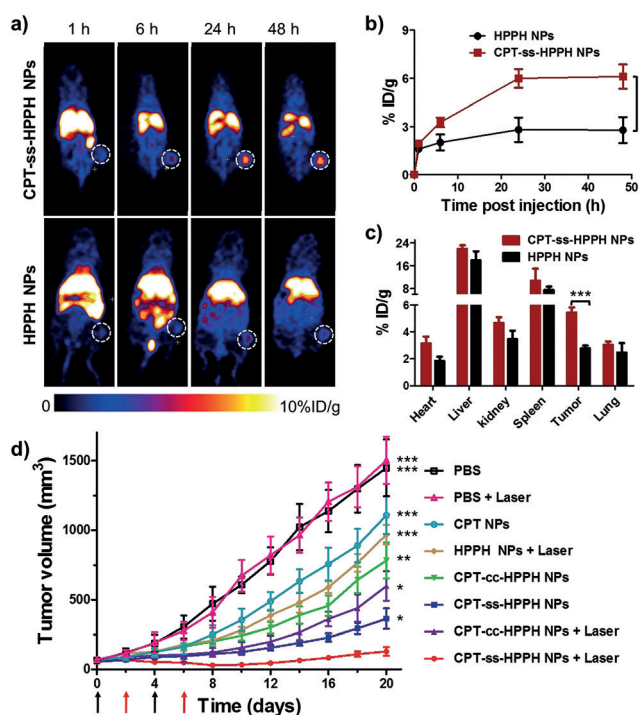


Figure 3. HDMP-loaded NPs enable efficient drug delivery to tumor and synergistic tumor chemotherapy and photodynamic therapy. a) Representative whole-body coronal PET images of HCT116 tumor-bearing mice intravenously injected with CPT-ss-HPPH NPs or HPPH NPs at different time points post injection. White circles mark the location of tumors. b) Drug accumulation in tumor quantified from decay-corrected PET images ($n=3$). c) Ex vivo drug distribution determined by γ -counting of excised organs at 48 h post injection ($n=3$). d) The tumor growth curves after treatment ($n=5$). Black arrows indicate intravenous injection of drugs; red arrows indicate laser irradiation. Asterisks mark the significant differences between CPT-ss-HPPH NPs and the other treatments. *: $p < 0.05$; **: $p < 0.01$; ***: $p < 0.001$.

premature release of CPT-ss-HPPH is also expected to reduce systemic toxicity after intravenous administration.

Encouraged by the promising *in vitro* cytotoxicity and *in vivo* drug delivery of CPT-ss-HPPH NPs, we further investigated these NPs for synergistic therapy on HCT116 tumor. Since PET imaging revealed highest tumor accumulation of CPT-ss-HPPH at 48 h post-injection, the mice were given intravenously two doses every 4 day, and the tumor was irradiated using 670 nm laser at 2 days following each injection for 10 min at 200 mW cm^{-2} . As shown in Figure 3d, while the tumor of mice treated with PBS or PBS + laser grew quickly, the treatment of CPT-ss-HPPH NPs with laser irradiation dramatically shrunk tumor volumes. In contrast, both CPT NPs and HPPH NPs showed limited tumor growth inhibition. Moreover, the significantly inferior tumor inhibition of CPT-cc-HPPH over CPT-ss-HPPH clearly demonstrated the necessity of GSH-cleavable disulfide linkage. Consistently, mice treated with CPT-ss-HPPH NPs showed the best survival over other treatment groups (Supporting Information, Figure S12). Besides, mice treated with CPT NPs displayed noticeable body weight reduction (6% at day 6; Supporting Information, Figure S13), whereas a maximum

of 2% body weight reduction in mice treated with CPT-ss-HPPH NPs was observed, which is most likely due to less premature drug release.

In summary, we have designed a GSH-responsive HDMP, which was efficiently loaded into polymeric nanocarrier and co-delivered two synergistic drugs to tumor, leading to favorable tumor therapy. The HDMP was prepared via a simple two-step reaction using commercially available reagents, and encapsulated into biocompatible PEG-*b*-PLA with high loading capacity and quantitative loading efficiency. Remarkably, these HDMP-based NPs demonstrated 10-fold slower premature drug release than the corresponding monomeric drug-loaded NPs. The disulfide linkage was essential for the on-demand drug release and maintaining effective cytotoxicities. Furthermore, the fluorogenicity nature and the ability of HPPH for direct radiolabeling allowed us to monitor *in vitro* cellular uptake of drugs by fluorescence microscopy and to study *in vivo* pharmacoinaging by PET imaging, which demonstrated that HDMP NPs significantly improved drug delivery to tumor. Finally, CPT-ss-HPPH NPs demonstrated synergistic tumor therapy efficacy by combining chemotherapy and photodynamic therapy. Overall, these results demonstrate HDMP is a promising approach for efficient and safe drug delivery in combination cancer therapy, and open up new opportunities to for drug delivery.

Acknowledgements

F.Z. and Q.N. contributed equally to this work. This research was supported by the Intramural Research Program of the NIBIB, NIH, and the National Key Basic Research Program of the People's Republic of China (2014CB744501 and 2014CB744504).

Conflict of interest

The authors declare no conflict of interest.

Keywords: dimeric prodrugs · drug delivery · nanomedicine · pharmacoinaging · synergistic therapy

How to cite: *Angew. Chem. Int. Ed.* **2018**, *57*, 7066–7070
Angew. Chem. **2018**, *130*, 7184–7188

- [1] a) S. Schöttler, K. Landfester, V. Mailander, *Angew. Chem. Int. Ed.* **2016**, *55*, 8806–8815; *Angew. Chem.* **2016**, *128*, 8950–8959; b) F. Jia, X. Lu, X. Tan, D. Wang, X. Cao, K. Zhang, *Angew. Chem. Int. Ed.* **2017**, *56*, 1239–1243; *Angew. Chem.* **2017**, *129*, 1259–1263.
- [2] C. Oerlemans, W. Bult, M. Bos, G. Storm, J. F. W. Nijssen, W. E. Hennink, *Pharm. Res.* **2010**, *27*, 2569–2589.
- [3] a) A. G. Cheetham, P. C. Zhang, Y. A. Lin, L. L. Lock, H. G. Cui, *J. Am. Chem. Soc.* **2013**, *135*, 2907–2910; b) M. Elsbahy, K. L. Wooley, *Chem. Soc. Rev.* **2012**, *41*, 2545–2561.
- [4] a) X. Y. Tan, B. B. Li, X. G. Lu, F. Jia, C. Santori, P. Menon, H. Li, B. H. Zhang, J. J. Zhao, K. Zhang, *J. Am. Chem. Soc.* **2015**, *137*, 6112–6115; b) S. Zhang, J. Zou, F. Zhang, M. Elsbahy, S. E. Felder, J. Zhu, D. J. Pochan, K. L. Wooley, *J. Am. Chem.*

- Soc.* **2012**, *134*, 18467–18474; c) F. Zhang, S. Khan, R. Li, J. A. Smolen, S. Zhang, G. Zhu, L. Su, A. A. Jahnke, M. Elsabahy, X. Chen, K. L. Wooley, *Nanoscale* **2017**, *9*, 15773–15777.
- [5] a) X. Guo, L. Wang, K. Duval, J. Fan, S. Zhou, Z. Chen, *Adv. Mater.* **2018**, *30*, 1705436; b) P. Huang, D. L. Wang, Y. Su, W. Huang, Y. F. Zhou, D. X. Cui, X. Y. Zhu, D. Y. Yan, *J. Am. Chem. Soc.* **2014**, *136*, 11748–11756.
- [6] a) K. M. Cai, X. He, Z. Y. Song, Q. Yin, Y. F. Zhang, F. M. Uckun, C. Jiang, J. J. Cheng, *J. Am. Chem. Soc.* **2015**, *137*, 3458–3461; b) L. Su, R. Li, S. Khan, R. Clanton, F. Zhang, Y.-N. Lin, Y. Song, H. Wang, J. Fan, S. Hernandez, A. S. Butters, G. Akabani, R. MacLoughlin, J. Smolen, K. L. Wooley, *J. Am. Chem. Soc.* **2018**, *140*, 1438–1446.
- [7] A. Srivatsan, M. Ethirajan, S. K. Pandey, S. Dubey, X. Zheng, T.-H. Liu, M. Shibata, J. Missert, J. Morgan, R. K. Pandey, *Mol. Pharm.* **2011**, *8*, 1186–1197.
- [8] a) Y. Q. Shen, E. L. Jin, B. Zhang, C. J. Murphy, M. H. Sui, J. Zhao, J. Q. Wang, J. B. Tang, M. H. Fan, E. Van Kirk, W. J. Murdoch, *J. Am. Chem. Soc.* **2010**, *132*, 4259–4265; b) H. Su, P. C. Zhang, A. G. Cheetham, J. M. Koo, R. Lin, A. Masood, P. Schiapparelli, A. Quinones-Hinojosa, H. G. Cui, *Theranostics* **2016**, *6*, 1065–1074.
- [9] a) C. Wigerup, S. Pahlman, D. Bexell, *Pharmacol. Ther.* **2016**, *164*, 152–169; b) D. Bertozzi, J. Marinello, S. G. Manzo, F. Fornari, L. Gramantieri, G. Capranico, *Mol. Cancer Ther.* **2014**, *13*, 239–248.
- [10] M. Hoebeke, X. Damoiseau, *Photochem. Photobiol. Sci.* **2002**, *1*, 283–287.
- [11] a) J. Siepmann, N. A. Peppas, *Adv. Drug Delivery Rev.* **2001**, *48*, 139–157; b) Y. Fu, W. J. Kao, *Expert Opin. Drug Delivery* **2010**, *7*, 429–444.
- [12] C. J. Kim, *Drug Dev. Ind. Pharm.* **1998**, *24*, 645–651.

Manuscript received: February 13, 2018

Revised manuscript received: March 16, 2018

Accepted manuscript online: April 6, 2018

Version of record online: May 14, 2018